ISSN (Print) 1226-1750
ISSN (Online) 2233-6656
Journal of Magnetics 26(1), 1-6 (2021) https://doi.org/10.4283/JMAG.2021.26.1.001

Tunable Domain Wall Chirality by Changing Co/Pt Multilayer Repeat Numbers

Lin Huang[1], Sang-Hyuk Lee[1,2], Nam-Hui Kim[3], Dae-Yun Kim[4,5], June-Seo Kim[6], Chun-Yeol You[3], Sug-Bong Choe[4], and Dong-Hyun Kim[1]*

[1]*Department of Physics, Chungbuk National University, Cheongju 28644, Republic of Korea*
[2]*Advanced Instrumentation Institute, Korea Research Institute of Standards and Science, Daejeon 34113, Republic of Korea*
[3]*Department of Emerging Materials Science, DGIST, Daegu 42988, Republic of Korea*
[4]*Department of Physics and Institute of Applied Physics, Seoul National University, Seoul 08826, Republic of Korea*
[5]*Center for Spintronics, Korea Institue of Science and Technology, Seoul 02792, Republic of Korea*
[6]*Division of Nanotechnology, DGIST, Daegu 42988, Republic of Korea*

(Received 5 December 2020, Received in final form 7 March 2021, Accepted 8 March 2021)

The chirality of a magnetic domain wall was modified in ultrathin ferromagnetic Co/Pt multilayer films by varying the repeat number *n*. Direct observations of field-driven asymmetric wall motion revealed a change in sign of the Dzyaloshinskii-Moriya interaction coefficient from positive (*n* = 1, 2, and 3) to negative (*n* = 4), implying the domain wall chirality changes from a left- to right-handed Néel wall. These findings provide a way to control the domain wall chirality in multilayers simply by changing the repeat numbers.

Keywords : Dzyaloshinskii-Moriya interaction, magnetic domain wall, domain wall chirality

1. Introduction

The Dzyaloshinskii-Moriya interaction (DMI) has attracted considerable attention owing to recent findings regarding the magnetic domain wall (DW) dynamics by controlling a DW [1, 2]. DMI emerges from interfacial two neighboring spins, $\vec{S}_1$ and $\vec{S}_2$, with strong spin-orbit coupling (SOC) with the Hamiltonian form, $H_{DMI} = -\vec{D}_{12} \cdot (\vec{S}_1 \times \vec{S}_2)$, where $\vec{D}_{12}$ is the DMI vector. The interfacial DMI induces a symmetry breaking by generating an effective in-plane magnetic field from a strong SOC, transforming the Bloch wall into the Néel wall structure, possibly leading to faster DW motion [3, 4]. Néel-like skyrmions are stabilized in thin films possessing an interfacial DMI, where symmetry breaks at the interface between a heavy metal (HM) and a ferromagnet (FM) bilayer with strong SOC [5-7]. DMI has also been studied extensively for HM_1/FM/HM_2 trilayer systems with an asymmetric thickness configuration between HM_1 and HM_2 [8-10]. In the case of a Pt/Co/AlO_x trilayer [11-13], the interfacial DMI effective field, $\mu_0 H_{DMI}$, acts as an effective in-plane field, breaking the rotational symmetry, hence stabilizing the Néel walls with fixed chirality, which is one of the key aspects in achieving reliable performance for novel spintronic devices [14-17] and racetrack memory devices [18].

On the other hand, various multilayer films with HM/FM interfaces have emerged as ideal candidates for developing such devices owing to the DMI strength tunability by varying the multilayer components and relative layer thicknesses [14, 15, 19]. The aforementioned efficient and faster DW motion boosted by interfacial DMI has been demonstrated experimentally in a variety of multilayer film systems. Moreover, the DMI coefficient D value could reach up to 2 mJ/m^2 for Pt/Co/Ir multilayers [20], in which asymmetric Pt and Ir layers result in an enhanced $\mu_0 H_{DMI}$. Chirality-tunable left- and right-handed Néel walls have been observed for Co/Ni multilayers [8, 19] and Pt/Co/Ir/Pt [9] with a variation of the components and the relative ratio of the layer thickness.

In addition to the variation of multilayer components and layer thickness, very little has been reported for the interfacial DMI behavior with a variation of the multilayer repeat numbers (n). Recently, there has been a report on the sign reversal of D with a variation of n for Co/Pd multilayer, sandwiched by Pt [21], was reported. The sign reversal from negative (n = 2) to positive (n = 3, 4, and 5) was attributed to the large positive contribution to D from

*Corresponding author: Tel: +82-43-261-2268
Fax: +82-43-274-7811, e-mail: donghyun@chungbuk.ac.kr

the Co/Pd multilayer structure. Interestingly, our experimental results reveal an opposite trend of positive D for the repeat number n smaller than 4 but a negative D for n = 4, clearly indicating showing that the interfacial DMI sign can be reversed by changing n. The Co/Pt multilayer system was selected because the Co/Pt interface provides a very high SOC among various FM/HM systems. D is determined by an analysis of purely field-driven DW motion to avoid complex interplays of spin-transfer torque [4], Rashba effect [22-24], and spin Hall effect [25, 26], allowing a straightforward interpretation. Sign reversal of D from positive (n = 1, 2, and 3) to negative (n = 4) in Co/Pt multilayers was observed, suggesting a change in DW chirality.

2. Experimental

The ferromagnetic thin films of Ta (3.0 nm)/Pt (3.0 nm)/[Pt (0.7 nm)/Co (0.5 nm)]$_n$/Pt (3.7 nm) multilayers (n = 1, 2, 3, and 4) with perpendicular magnetic anisotropy, as shown in Fig. 1(a), were fabricated on a glass substrate by DC magnetron sputtering with the base pressure of 3×10^{-8} Torr and Ar ion pressure of 1 mTorr. The magnetic hysteresis curve and saturation magnetization were measured using a vibrating sample magnetometer. The field-induced magnetic DW motion was observed directly using a magnet-optical Kerr effect (MOKE) microscope [27, 28]. A slightly tilted external magnetic field with a tilting angle of 2° from the sample plane was applied so that a weak out-of-plane (OOP) ($\mu_0 H_z$) and strong in-plane (IP) field ($\mu_0 H_x$) are applied to the samples, as shown in Fig. 1(b). The domain patterns were recorded using a CCD camera with 30 frames/sec, and consecutive domain images were processed to analyze the DW displacement.

3. Results and Discussion

For all the films, perpendicular magnetic anisotropy

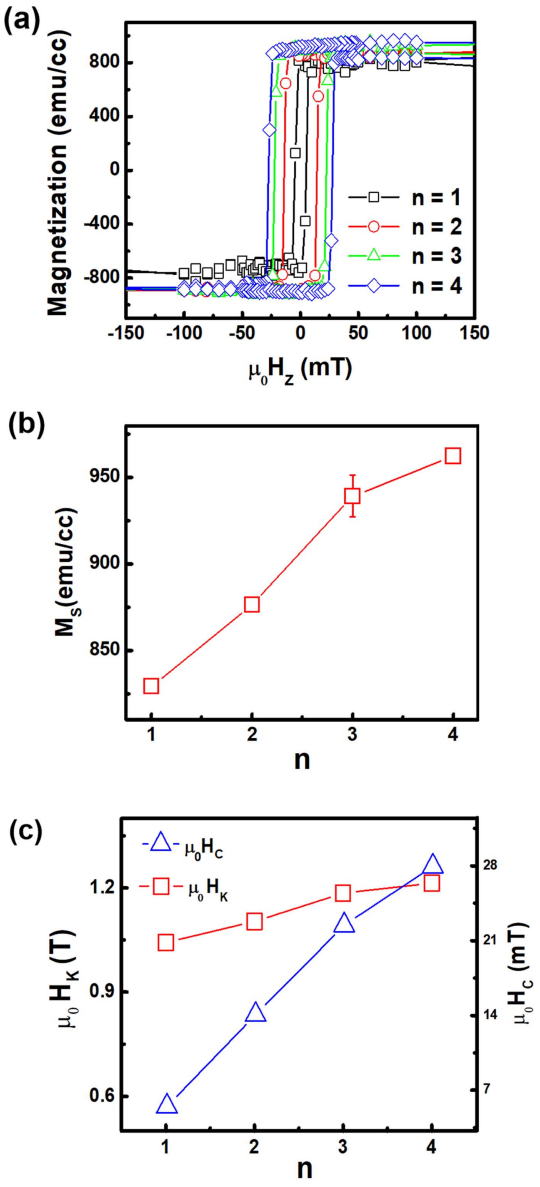

Fig. 2. (Color online) (a) OOP hysteresis loops measured by the vibrating sample magnetometer for n = 1, 2, 3, and 4. (b) Saturation magnetization M_s with respect to n. (c) Anisotropy field $\mu_0 H_K$ and coercivity field $\mu_0 H_c$ with respect to n.

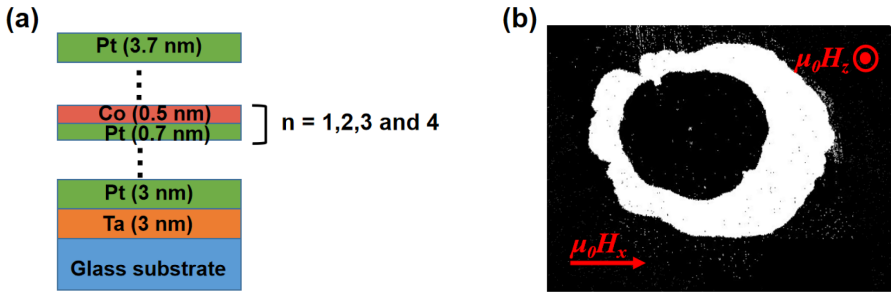

Fig. 1. (Color online) (a) Schematic diagram of the Co/Pt multilayer films with the variation of n, prepared on a glass substrate. A 3 nm Ta underlayer and 3.7 nm Pt capping layer were deposited. (b) Example of a DW image with the external field directions of the OOP ($\mu_0 H_z$) and IP ($\mu_0 H_x$).

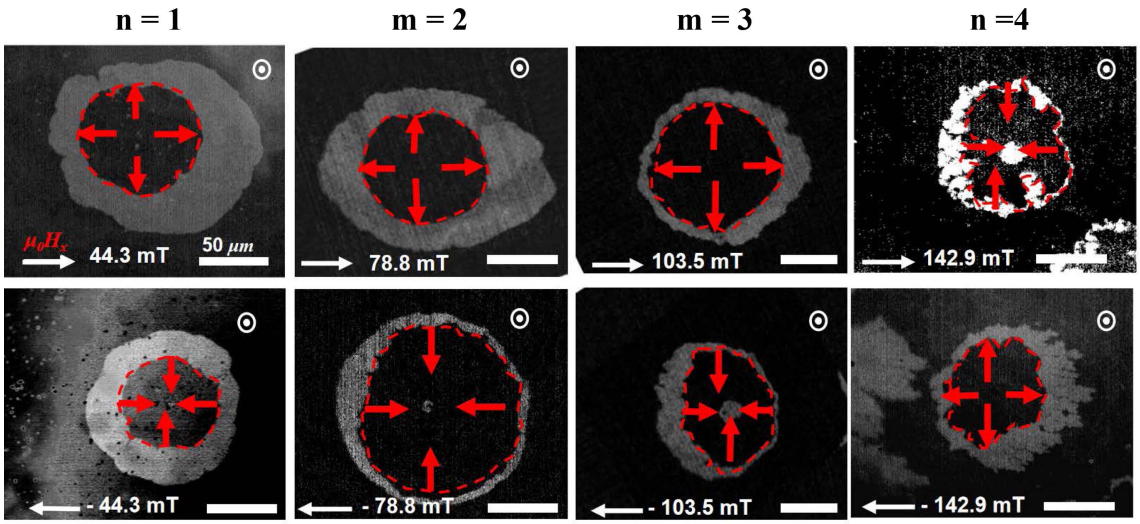

Fig. 3. (Color online) Anisotropic DW expansion at μ_0H_x under positive (upper row) and negative (lower row) direction. The external field strength and direction are commented on in each picture. The red dotted circular pattern denotes an initially prepared DW by OOP μ_0H_z, which is expanded with the direction along the red arrows.

was confirmed from the hysteresis curve along the OOP direction, as shown in Fig. 2(a), where all the films exhibit perfect squareness. The saturation magnetization (M_s) increases slightly with increasing n, as shown in Fig. 2(b). The magnetic anisotropy field (μ_0H_K) and coercivity (μ_0H_c) were determined from the hysteresis loop measurements (Fig. 2(c)). The anisotropy increased almost proportionally with n, whereas the μ_0H_k value increased slightly with n, but was around 1 *T*. The increase in μ_0H_c with n might have some association with the anisotropy enhancement, as observed in the figure. Although M_s increases with n, μ_0H_K showed a rather insensitive variation with the change in n. Thus, with larger n, magnetic domains with a rather complex structure are expected. As expected, the domain patterns for the sample with n = 1 were relatively smooth, but became substantially rugged with n = 4 [29], as shown in Fig. 3. Quantitative analysis of the domain structure complexity was performed based on fractal analysis [30] or roughness analysis [31]. In the present case, the roughness exponent increased with increasing n.

To investigate the DW propagation behavior, an OOP field (μ_0H_z) was applied to generate a circular domain. The dotted red line represents the initial domain patterns prepared by μ_0H_z, where the overall symmetric patterns were sustained. The IP field (μ_0H_x) was applied to drive an asymmetric DW motion. As shown in the figure, the breaking of rotational symmetry in the domain patterns was observed. The DW moved either parallel (n = 1, 2, and 3) or antiparallel (n = 4) to μ_0H_x. In the case of a positive μ_0H_x (upper row in the figure), the DW moved to the right, parallel to the direction of H_x for n = 1, 2, and 3, whereas DW moved to the left, antiparallel to the direction of H_x for n = 4. A similar trend was observed in the case of a negative μ_0H_x (bottom row in the figure). For n = 4, the DW expansion behavior with μ_0H_x showed the pinning potential [32-34], local pinning of the crack front during DW propagation, which is the roughness of the fracture surfaces left by the crack, as shown in Fig. 3. This implies the existential role of the pinning sites, and the number of pinning sites might be proportional to the repeat number n. However, even with the possible change in pinning site numbers, domain wall creep behavior still exhibits a strong universality.

The analysis was carried out to determine the DMI coefficient D for these samples from the directly observed domain patterns [9, 35]. The DW velocity, v, versus μ_0H_x with various n values was plotted on a log-normal scale (Fig. 4(a)). v was measured by detecting the DW displacement at the rightmost or leftmost of the circular domain. v is described as [35]

$$v = v_0 \exp[-\varsigma(\mu_0 H_z)^{-\mu}] \quad (1),$$

where μ is the creep scaling exponent, and v_0 is the characteristic speed. ζ is the scaling coefficient expressed as $\varsigma = \varsigma_0[\sigma(H_x)/\sigma_0]^{1/4}$, where ζ_0 is the scaling fitting parameter and σ is the DW energy density as a function of μ_0H_x [9, 35], as follows:

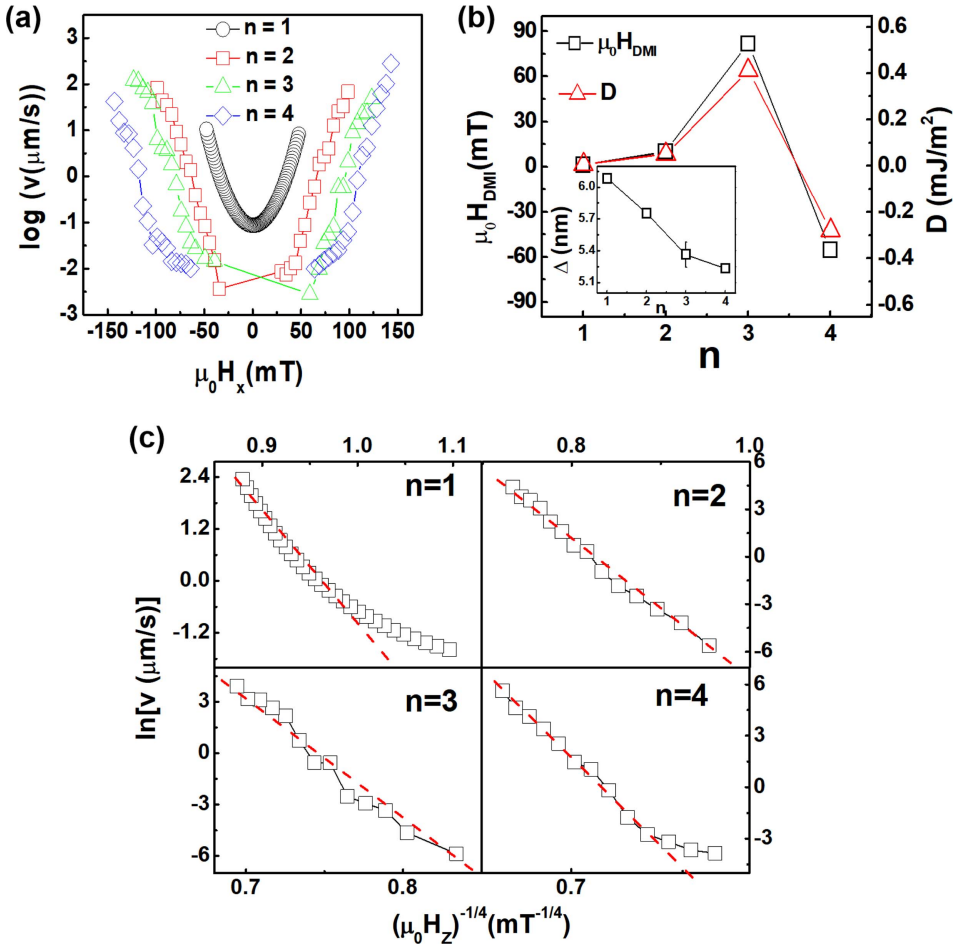

Fig. 4. (Color online) (a) Log-normal of DW velocity as a function of $\mu_0 H_x$ for n = 1, 2, 3, and 4. (b) $\mu_0 H_{DMI}$ and D with respect to n. Inset shows the DW width Δ with respect to n. (c) $ln(v)$ vs. $(\mu_0 H_z)^{-1/4}$ for n = 1, 2, 3, and 4. The dashed lines are for guide.

$$\sigma(H_x) = \begin{cases} \sigma_0 - \dfrac{\pi^2 \Delta M_S^2}{8K_D}(\mu_0 H_x + \mu_0 H_{DMI})^2 \\ \sigma_0 + 2K_D\Delta - \pi\Delta M_S\left|\mu_0 H_x + \mu_0 H_{DMI}\right| \end{cases}$$

$$for \left|\mu_0 H_x + \mu_0 H_{DMI}\right| < \frac{4K_D}{\pi M_S} \qquad (2)$$

σ_0 is the Bloch wall energy density, and K_D is the DW anisotropy energy density. Δ is the DW width, where $\Delta = \sqrt{A/K_{eff}}$ for the exchange stiffness constant, A, and the effective anisotropy constant, K_{eff}. If the combined effective field of $\mu_0 H_x$ and $\mu_0 H_{DMI}$ is not strong enough to fully transform the Bloch to Néel wall, as in the case of $\left|\mu_0 H_x + \mu_0 H_{DMI}\right| < \frac{4K_D}{\pi M_S}$, the mixed Bloch and Néel DW energy density can be described as the former one. If $\left|\mu_0 H_x + \mu_0 H_{DMI}\right| > \frac{4K_D}{\pi M_S}$, σ becomes a simple sum of the four contributions (Bloch wall energy density, DW anisotropy energy density, Zeeman energy density, and DMI).

Figure 4(b) presents the determined DMI effective field $\mu_0 H_{DMI}$ values. The creeping behavior of DW was also confirmed (Fig. 4(c)), where the dotted lines are used as a guide for the creep scaling exponent μ = 1/4.

From the relation, $\mu_0 H_{DMI} = D / M_s\Delta$, $\mu_0 H_{DMI}$ and D are expected to have a similar trend, as shown in Fig. 4(b). The inset figure shows that the DW width, Δ, decreases monotonically with n, which is consistent with the monotonic increase in the anisotropy field (Fig. 2(c)). The D value changed with n; it increased from 0.006 (n = 1) to 0.412 mJ/m^2 (n = 3), but decreased to - 0.279 mJ/m^2 (n = 4) with a sign change, which again reflects the difference in asymmetric DW motion observed in Fig. 3. The sign change suggests the DW chirality modification from the left- to right-hand Néel DW. For positive (negative) $\mu_0 H_{DMI}$ over the Bloch-Néel wall transition region limit, DMI stabilizes the chirality with the left-hand (right-hand) Néel wall as in the case of n = 1, 2, and 3 (n = 4).

With increasing M_s and thus, the dipolar interaction

with respect to n (Fig. 2), the domain pattern can be more striped-like than simple circular-like. On the other hand, the wall energy might also increase because of the increasing $\mu_0 H_k$ (Fig. 4(b)), costing more energy in the generation of a complex pattern of a domain wall configuration. This implies the existential role of pinning sites, as the number of pinning sites might be proportional to the repeat number n. On the other hand, even with the change in pinning site numbers, the asymmetric shift of the domain wall velocity in the domain wall creep region (Fig. 4) is still valid because of the strong universality in the creeping behavior. Therefore, the observed sign change of the effective DMI might not be explained simply based on any models assuming the pinning potential energy landscape experienced by the domain wall with elastic tension.

Considering that the chirality change is eventually involved with the SOC at the interfaces of multilayers, it might be affected by the effective Pt layer thickness of the present samples. The bottom Pt layer thickness (t_{Pt}) was fixed to 3.7 nm. On the other hand, the second Co layer has the neighboring underlayer, t_{Pt}, of 0.7 nm in addition to the bottom Pt. Thus, the effective underlayer, t_{Pt}, might be approximated to $[3.7 + 0.7\ (n - 1)]/n$, effectively modifying the interfacial SOC with n. For n = 1, 2, 3, and 4, the effective t_{Pt} was 3.7, 2.2, 1.7, and 1.65, respectively. Note that the number is similar for the cases of n = 3 and 4. The change in sign is not simple to explain, considering that the anisotropy field and saturation magnetization, as well as the DW width, change monotonically with respect to n. One possibility is that the spin structure becomes three-dimensional as n increases, as suggested recently by theoretical calculations, where the three-dimensional texture of the stacked spin spiral might exist for a certain thickness range [36]. If the spin texture is sustained as two-dimensional, another possible explanation would be a chiral damping phenomenon, which could also help determine the DMI [37-39]. Therefore, the amplitude and sign of the D values determined by DMI-based analysis might not be sufficient and exact if the chiral damping effect or three-dimensional stacked spin texture exists, which might be encountered in many cases of multilayers. The development of a comprehensive analysis model for asymmetric DW motion, considering the possible mechanisms is needed.

4. Conclusions

The DW chirality can be modified by changing n while fixing the other multilayer parameters in Co/Pt multilayers. It has been found that the sign of D has been changed as the multilayer repeat number increases from 1 to 4, which might allow a control of the DW chirality with a DW inner structure transition between the left- and right-handed Néel walls simply by changing n. This provides a practical way to modify the DW chirality in spintronic devices based on the number of ferromagnetic multilayers.

Acknowledgments

This study was supported by the National Research Foundation of Korea (NRF) [Grant No. 2018R1A2B3009569] and by a KBSI Grant D39614. This work was also supported in part by Global Research Laboratory Program [Grant No 2009-00439] and by Max Planck POSTECH/ KOREA Research Initiative Program [Grant No 2016K1A4A4A01922028] through the National Research Foundation of Korea (NRF) funded by Ministry of Science, ICT & Future Planning. D.-Y. K. and S.-B. C. were supported by the Samsung Science & Technology Foundation [SSTF-BA1802-07]. D.-Y. Kim was supported by the KIST institutional program [grant no. 2E29410] and National Research Council of Science & Technology [grant no.CAP-16-01-KIST].

References

[1] I. Dzyaloshinsky, J. Phys. Chem. Solids **4**, 241 (1958).
[2] T. Moriya, Phys. Rev. **120**, 91 (1960).
[3] D.-H. Kim, D.-Y. Kim, S.-C. Yoo, B.-C. Min, and S.-B. Choe, Phys. Rev. B **99**, 134401 (2019).
[4] E. Martinez, S. Emori, and G. S. D. Beach, Appl. Phys. Lett. **103**, 072406 (2013).
[5] K.-W. Kim, H.-W. Lee, K.-J. Lee, and M. D. Stiles, Phys. Rev. Lett. **111**, 216601 (2013).
[6] M. Heide, G. Bihlmayer, and S. Blügel, Phys. Rev. B **78**, 140403(R) (2008).
[7] H. Yang, A. Thiaville, S. Rohart, A. Fert, and M. Chshiev, Phys. Rev. Lett. **115**, 267210 (2015).
[8] G. Chen, A. T. N'Diaye, Y. Wu, and A. K. Schmid, Appl. Phys. Lett. **106**, 062402 (2015).
[9] A. Hrabec, N. A. Porter, A. Wells, M. J. Benitez, G. Burnell, S. McVitie, D. McGrouther, T. A. Moore, and C. H. Marrows, Phys. Rev. B **90**, 020402(R) (2014).
[10] J. Cho, N.-H. Kim, S.-K. Kang, H.-K. Hwang, J. Jung, H. J.-M. Swagten, J.-S. Kim, and C.-Y. You, Jour. of Phys. D: Appl. Phys. **50**, 425004 (2017).
[11] M. J. Benitez, A. Hrabec, A. P. Mihai, T. A. Moore, G. Burnell, D. McGrouther, C. H. Marrows, and S. McVitie, Nat. Commun. **6**, 8957 (2015).
[12] J. H. Franken, M. Herps, H. J. M. Swagten, and B. Koopmans, Sci. Rep. **4**, 5248 (2014).
[13] D.-S. Han, N.-H. Kim, J.-S. Kim, Y. Yin, J.-W. Koo, J.

Cho, S. Lee, M. Kläui, H. J. M. Swagten, B. Koopmans, and C.-Y. You, Nano Lett. **16**, 4438 (2016).
[14] J. Yu, X, Qiu, Y. Wu, J. Yoon, P. Deorani, J. M. Besbas, A. Manchon, and H. Yang, Sci. Rep. **6**, 32629 (2016).
[15] X. Ma, G. Yu, C. Tang, X. Li, C. He, J. Shi, K. L. Wang, and X. Li, Phys. Rev. Lett. **120**, 157204 (2018).
[16] Z. Wang, B. Zhang, Y. Cao, and P. Yan, Phys. Rev. Appl. **10**, 054018 (2018).
[17] Y. Zhou, Nat. Sci. Rev. **6**, 210 (2019).
[18] S. S. P. Parkin, M. Hayashi, and L. Thomas, Science **320**, 190 (2008).
[19] G. Chen, T. Ma, A. T. N'Diaye, H. Kwon, C. Won, Y. Wu, and A. K. Schmid, Nat. Commun. **4**, 2671 (2013).
[20] C. Moreau-Luchaire, C. Moutafis, N. Reyren, J. Sampaio, C. A. F. Vaz, N. Van Horne, K. Bouzehouane, K. Garcia, C. Deranlot, P. Warnicke, P. Wohlhüter, J.-M. George, M. Weigand, J. Raabe, V. Cros, and A. Fert, Nat. Nanotechnol. **11**, 444 (2016).
[21] S. D. Pollard, J. A. Garlow, J. Yu, Z. Wang, Y. Zhu, and H. Yang, Nat. Commun. **8**, 14761 (2017).
[22] K. Obata and G. Tatara, Phys. Rev. B **77**, (2008) 214429.
[23] I. M. Miron, T. Moore, H. Szambolics, L. D. B.-Prejbeanu1, S. Auffret. B. Rodmacq, S. Pizzini, J. Vogel, M. Bonfim, A. Schuhl, and G. Gaudin, Nat. Mater. **10**, 419 (2011).
[24] K.-W. Kim, S.-M. Seo, J. Ryu, K.-J. Lee, and H.-W. Lee, Phys. Rev. B **85**, 180404(R) (2012).
[25] K. Garello, I. M. Miron, C. O. Avci, F. Freimuth, Y. Mokrousov, S. Blügel, S. Auffret, O. Boulle, G. Gaudin, and P. Gambardella, Nat. Nanotechnol. **8**, 587 (2013).
[26] L. Liu, C.-F. Pai, Y. Li, H. W. Tseng, D. C. Ralph, and R. A. Buhrman, Science **336**, 555 (2012).
[27] D.-H. Kim, S.-B. Choe, and S.-C. Shin, Phys. Rev. Lett. **90**, 087203 (2003).
[28] D.-T. Quach, D.-T. Pham, D.-T. Ngo, T.-L. Phan, S.-Y. Park, S.-H. Lee, and D.-H. Kim, Sci. Rep. **8**, 4461 (2018).
[29] L. Fallarino, A. Oelschlägel, J. A. Arregi, A. Bashkatov, F. Samad, B. Böhm, K. Chesnel, and O. Hellwig, Phys. Rev. B **99**, 024431 (2019).
[30] D.-H. Kim, Y.-C. Cho, S.-B. Choe, and S.-C. Shin, Appl. Phys, Lett. **82**, 3698 (2003).
[31] K.-S. Lee, C.-W. Lee, Y.-J. Cho, S. Seo, D.-H. Kim, and S.-B. Choe, IEEE Trans. Magn. **45**, 2548 (2009).
[32] J. M. Knut, S. Stéphane, S. Jean, and T. Renaud, Phys. Rev. Lett. **96**, 045501 (2006).
[33] D. M. F. Hartmann, R. A. Duine, M. J. Meijer, H. J. M. Swagten, and R. Lavrijsen, Phys. Rev. B **100**, 094417 (2019).
[34] P. J. Metaxas, P.-J. Zermatten, R. L. Novak, S. Rohart, J.-P. Jamet, R. Weil, J. Ferre, A. Mougin, R. L. Stamps, G. Gaudin, V. Baltz, and B. Rodmacq, J. Appl. Phys. **113**, 073906 (2013).
[35] S.-G. Je, D.-H. Kim, S.-C. Yoo, B.-C. Min, K.-J. Lee, and S.-B. Choe, Phys. Rev. B **88**, 214401 (2013).
[36] F. N. Rybakov, A. B. Borisov, S. Blügel, and N. S. Kiselev, New J. Phys. **18**, 045002 (2016).
[37] E. Jué, C. K. Safeer, M. Drouard, A. Lopez, P. Balint, L. B-Prejbeanu, O. Boulle, S. Auffret, A. Schuhl, A. Manchon, I. M. Miron, and G. Gaudin, Nature Mater. **15**, 272 (2016).
[38] D.-Y. Kim, M.-H. Park, Y.-K. Park, J. S. Kim, Y.-S. Nam, D.-H. Kim, S.-G. Je, H.-C. Choi, B.-C. Min, and S.-B. Choe, NPG Asia Mater. **10**, e464 (2018).
[39] K.-W. Kim and H.-W. Lee, Nature Mater. **15**, 253 (2016).